Effects of Cryo-Milling and Milling Time on the Microstructures of Oxide-Dispersion Strengthened CoCrFeMnNi High-Entropy Alloy Powder

SeungHyeok Chung, Ho Jin Ryu *,
Department of Nuclear & Quantum Engineering, Korea Advanced Institute of Science and Technology, 291 Daehakro, Yuseong, 34141, Republic of Korea
**Corresponding author: hojinryu@kaist.ac.kr*

1. Introduction

High Entropy Alloys (HEAs) have more than 5 metallic principal elements with an equiatomic ratio or near equiatomic ratio [1]. HEAs exhibit excellent mechanical properties [3, 4] due to the following characteristics: High configurational entropy, lattice distortion, sluggish diffusion and cocktail effect [2]. Therefore HEAs appear to be a promising material for applications which require the excellent mechanical properties.

Despite the excellent mechanical properties of HEAs, improving HEAs is inevitable to expand the utilization areas of HEAs. Especially, the irradiation performance of HEAs is not established clearly yet [5]. To maintain the structural and compositional stability under irradiation, dispersing the nano-sized oxide particles in HEAs has been considered [5-7]. The oxide-dispersion strengthened steels (ODSs) are usually manufactured by the complicated process. Mechanical alloying (MA) is usually using for fabricating the ODS to disperse the nano-sized oxide particles homogeneously and make the size of particles very fine [8]. The mechanically alloyed powder subsequently consolidated by hot isostatic pressing (HIP) or spark plasma sintering (SPS) to obtain fully dense material in the required shape and promote the forming of nano-sized oxide particles within the matrix. However, the MA process has some drawbacks such as the time- and cost-consuming process, contamination from milling media, oxidation due to the friction heat during the MA [9].

CoCrFeMnNi HEA, which is called as Cantor alloy, is generally known as a model HEA. It shows a single phase with a simple FCC structure and exhibits both excellent ductility and fracture toughness even at a cryogenic temperature [10]. To understand the oxide dispersion strengthening mechanism of the HEA matrix, CoCrFeMnNi FCC HEA was chosen for this study.

In the present study, to clarify the milling parameters such as milling time and milling temperature, cryo-milling is selected as a method of MA. Microstructural characterization is conducted to understand the forming mechanisms of the nano-sized oxide particles at the powder preparing stage.

2. Experimental procedures

2.1 Powder preparation

CoCrFeMnNi HEA powder was manufactured by gas atomization. A mixture of Co, Cr, Fe, Mn, and Ni was induction melted under a high purity Ar atmosphere. The delivered molten metal was distributed by high pressured Ar gas and changed into the powder which has a different size range. The powder was sieved and separated into different size range from 32 (500 mesh) μm to 2 (10 mesh) mm. 0.5wt% of Y_2O_3 was added to form the nano-sized oxide particles before starting the MA. To investigate the milling temperature effect during the cryo-milling process, the atomized powder was subsequently cryo-milled in an attritor ball mill at -180℃ in a high purity Ar atmosphere using stainless steel vessels and balls as grinding media. The milling temperature has the control error range of ±10℃. To lower the temperature to the target temperature for cryo-milling, liquid nitrogen was injected into the space between the inner vessel and outer vessel. Therefore, the powder in the inner chamber was not contacted with liquid nitrogen directly. The cryo-milling was operated with a rotational speed of 200 rpm and a ball-to-powder ratio (BPR) of 10:1. The cryo-milling was conducted for 0.5, 1, 4, 10 and 24 hours respectively to investigate the milling time effect on Y_2O_3 added CoCrFeMnNi HEA powder. To understand the nano-sized oxide particle forming mechanisms during the consolidation process, the cryo-milled powder was annealed in the box furnace under high purity Ar condition. The annealing was performed at 900℃ for 1 h.

2.2 Characterization

The gas-atomized and cryo-milled powders were characterized by various methods such as x-ray diffraction (XRD), scanning electron microscopy (SEM), inductively coupled plasma (ICP) and transmission electron microscopy (TEM). The X-ray diffraction analysis was conducted using an XRD (Rigaku Smartlab) with Cu K_α radiation (λ =0.15406 nm) in θ-2θ configuration. 5°/min for scan speed and 0.01° for step size were used for the measurement. SEM (FEI Magellan400) was used for investigating the surface morphology and structural change of powder as milling time and temperature is increasing. The chemical compositions of gas-atomized and as-milled powders were determined using ICP-MS (Agilent ICP-MS 7700S) was used. TEM samples of cryo-milled powder were created by FIB (FEI Helios G4) milling. First, the mixed solution of cryo-milled powder and ethyl alcohol was deposited on the Si wafer. Secondly, the cryo-milled

powder on the Si wafer was milled by Ga ion beam. TEM (FEI Talos F200X) equipped with a high angle annular dark field (HAADF) detector. The energy dispersed X-ray spectroscopy (EDX) was performed in STEM mode.

3. Results and discussion

3.1 Chemical analysis

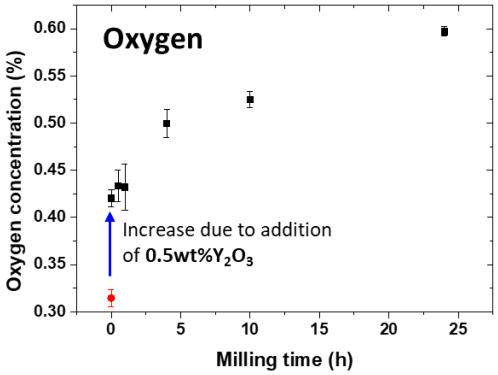

Fig. 1. The oxygen concentration of HEA and ODS-HEA powder versus milling time

The oxidation concentration is determined using determinator (ELTRA ONH-2000). As 0.5wt% of Y_2O_3 is added into CoCrFeMnNi HEA, about 0.101% of oxygen concentration is increased. The oxygen concentration is increasing as milling time increases. Even though the high purity Ar atmosphere and cryogenic temperature suppress the oxidation during the milling process, oxidation slightly occurs during the cryo-milling process. After the 24 h cryo-milling, about 0.18% of oxygen concentration is increased as shown in Fig. 1.

Table I: Chemical composition of the gas-atomized and cryo-milled powder

		Chemical composition (wt%)					
		Cr	*Co*	*Fe*	*Mn*	*Ni*	*Y*
Gas-atomized		18.23	18.62	19.98	21.85	21.03	0.29
As-milled	0.5 h	18.05	18.65	19.75	22.17	21.07	0.32
	1 h	18.28	18.32	20.08	21.95	21.08	0.28
	4 h	18.30	18.36	19.97	21.80	21.22	0.34
	10 h	17.40	19.50	19.70	21.30	21.50	0.29
	24 h	17.50	19.30	20.30	21.00	21.50	0.38

The chemical composition of gas-atomized and cryo-milled powder is summarized in Table I. It should be noted that the chemical composition of powders is maintained as an HEA composition during the cryo-milling process.

3.2 Powder morphology evolution

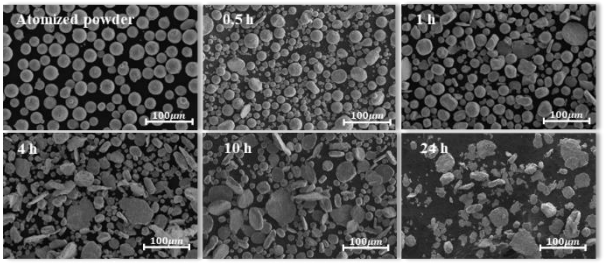

Fig. 2. The powder morphology evolution during the cryo-milling

The morphology evolution of 0.5wt% of Y_2O_3 added CoCrFeMnNi HEA powder during the cryo-milling process is shown in Fig. 2. The morphology of gas-atomized powder has fully sphere shape. As milling time increases, the sphere shape powders are transformed into the plate-shape. The plate-shaped powders are agglomerated and folded each other. After 24 h of cryo-milling, plate shape particles are split into the very fine particle.

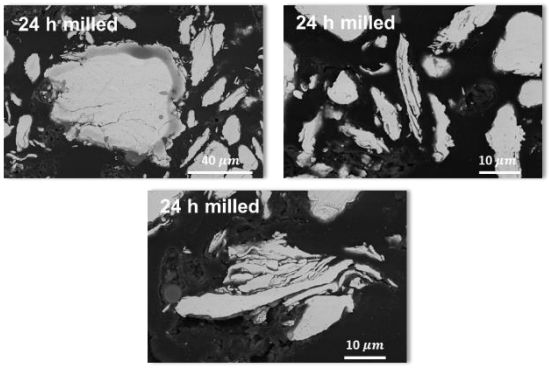

Fig. 3. The cross-sectional images of 0.5wt% of Y_2O_3 added CoCrFeMnNi after 24 h cryo-milling.

Fig. 3 shows cross-sectional SEM images of 0.5wt% of Y_2O_3 added CoCrFeMnNi HEA powder after 24 h cryo-milling. Since CoCrFeMnNi HEA has excellent ductility at the cryogenic temperature, particles are heavily deformed and welded together. The particles are folded each other and thus show a lamellar-like structure as shown in the Fig. 3. The long milling time makes particles fractured after the welding. Therefore, we can recognize the cold welding, fracturing, and re-welding processes are repeated during the cryo-milling process.

3.3 Microstructural analysis

3.3.1 XRD analysis

X-ray diffraction analysis was conducted to estimate the average grain size and dislocation density as a function of milling time. Fig. 4 shows XRD diffraction patterns of gas-atomized and cryo-milled powders. The blue circles and black diamonds indicate the Y_2O_3 peaks and CoCrFeMnNi HEA peaks respectively. Since Y_2O_3

was added only to 0.5wt%, Y_2O_3 diffraction peaks are very tiny on the whole XRD diffraction patterns. It was found in Fig. 4. That with an increase of milling time, the diffraction peaks of Y_2O_3 are decreasing and finally disappear after 4 h of cryo-milling. The intensities of diffraction peaks decrease and the broadening of diffraction peaks occurs as milling time increases. The broadening is attributed to simultaneous grain size and lattice strain [11].

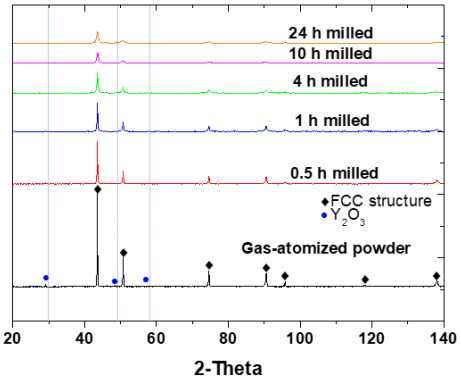

Fig. 4. X-ray diffraction patterns of 0.5wt% of Y_2O_3 added CoCrFeMnNi HEA powder mixture and after being mechanically milled for the various time

Grain size (D) and strain(ϵ) were estimated from the full width at half maximum (FWHM) using Halder-Wagner method [12]:

$$\frac{\beta^2}{tan^2\,\theta} = \frac{K\lambda}{D}\frac{\beta}{tan\theta sin\theta} + 16\epsilon^2 \quad (1)$$

Where K is the shape factor and β is the FWHM. The diffracted peaks were corrected with reference CoCrFeMnNi HEA powder for the broadening caused by the instrument itself. The reference CoCrFeMnNi HEA power was fully annealed at -1000℃ for 24 hours. The real broadening of CoCrFeMnNi HEA powder was calculated by the following equation:

$$(\beta_{exp}^2 - \beta_{inst}^2)^{1/2} = \beta \quad (2)$$

Where β_{exp} is the FWHM of the measured diffraction peak, β_{inst} is the FWHM of fully annealed CoCrFeMnNi HEA powder, and β is the real peak broadening of powder. The form of peaks is assumed as a Gaussian distribution.

The dislocation density was calculated by the following equation [13]: Where ϵ is the strain and b is the Burgers vector.

$$\rho = 14.4\left(\frac{\epsilon}{b}\right)^2 \quad (3)$$

The calculated grain size and dislocation density for various milling time are shown in Fig. 5. At the initial stage of cryo-milling, the grain refinement occurred rapidly and saturated to the particular value with slow variation as milling time increases. During the cryo-milling process, work hardening continuously occurs which may generate dislocation. After the 24 hours, cryo-milling the grain size and dislocation density are about 10 μm and $1.0 \times 10^{16}\mathrm{m}^{-2}$ respectively.

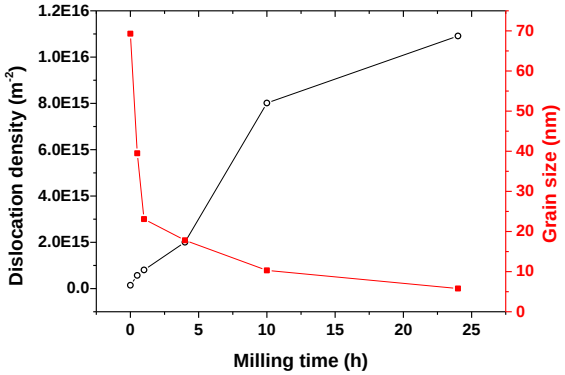

Fig. 5. Estimated grain size and dislocation density of 0.5wt% of Y_2O_3 CoCrFeMnNi HEA powder milled for various milling time

3.3.2 Electron microprobe analysis

The calculated grain sizes were double checked with TEM images. Fig. 6 shows the TEM image and magnified high-resolution image of 0.5wt% of Y_2O_3 added CoCrFeMnNi HEA powder. It indicates the grain sized of cryo-milled powder for 1 h become near 20 nm due to severe plastic deformation during cryo-milling. The estimated grain sizes from TEM image have consistent value with the calculated value from XRD diffracted peaks broadening.

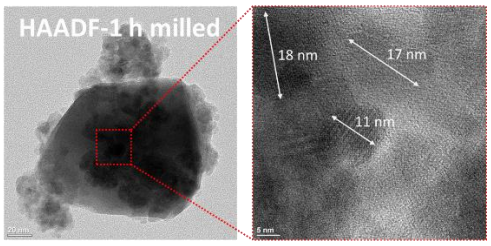

Fig. 6. TEM high-angle annular dark-field (HAADF) image and high resolution magnified image of 0.5wt% of Y_2O_3 added CoCrFeMnNi HEA powder milled for 1 h.

Fig. 7 shows TEM images of 0.5wt% of Y_2O_3 added CoCrFeMnNi HEA powder milled for 24 h and its EDX mapping for Y and O. EDX (Fig. 7a) mapping images of cryo-milled powder for 24 h indicate that the region where Y and O are distributed in the matrix is quite localized. Therefore, longer milling time or high energy for milling is necessary to achieve complete mechanical alloying.

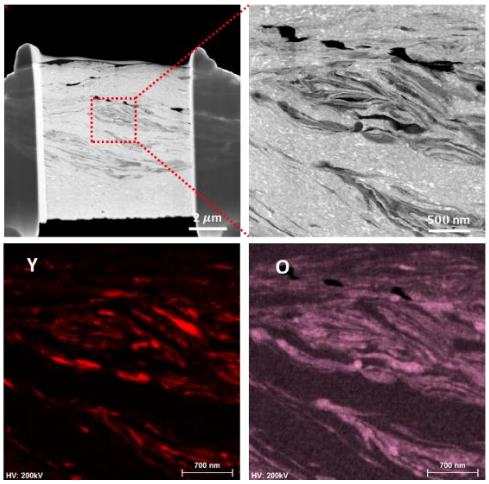

Fig. 7. TEM high-angle annular dark-field (HAADF) image and energy dispersed X-ray spectrometer (EDX) mapping image of 0.5wt% of Y_2O_3 added CoCrFeMnNi HEA powder cryo-milled for 24 h.

4. Conclusion

The 0.5wt% of Y_2O_3 added CoCrFeMnNi HEA powder was fabricated using cryo-milling under a high purity Ar atmosphere. Microstructural characterization was conducted to verify the effects of milling time and cryo-milling temperature on 0.5wt% of Y_2O_3 added CoCrFeMnNi HEA powder. The present research resulted in the following conclusions:

1. The chemical compositions were measured with ICP-MS. The chemical composition of 0.5wt% of Y_2O_3 added CoCrFeMnNi HEA powders was maintained as an ODS-HEA chemical composition during the cryo-milling process. However, the oxygen concentration was increased as milling time increases. As the milling time increases, the reaction area of powder increases and the reaction time increases, thus the oxygen concentration increases.
2. The grain size was calculated by broadening of diffracted peaks and double checked with TEM images of the cryo-milled powder. The grain sizes from XRD and TEM were quite well consistent with each other. The dislocation density was calculated using the value of strain from diffracted peak broadening.
3. The cryo-milled powder for 24 h shows the Y-enriched region was detected on the cryo-milled powder by TEM. It means that longer milling time or higher energy is necessary to achieve complete mechanical alloying of ODS-HEA.

ACKNOWLEDGMENT

The authors gratefully acknowledge the financial support provided by the Agency for Defense Development under the contract 1415156504.

REFERENCES

[1] Y. F. Ye, Q. Wang, J. Lu, C. T. Liu, and Y. Yang, “High-entropy alloy: challenges and prospects,” Mater. Today, vol. 19, no. 6, pp. 349–362, 2016.
[2] C. Zhang, M. C. Gao, and J.-W. Yeh, *High-Entropy Alloys: Fundamentals and Applications*. 2016.
[3]P.-K. Huang, J.-W. Yeh, T.-T. Shun, and S.-K. Chen, “Multi-Principal-Element Alloys with Improved Oxidation and Wear Resistance for Thermal Spray Coating,” *Adv. Eng. Mater.*, vol. 6, no. 12, pp. 74–78, 2004.
[4] C. Hsu, J. Yeh, S. Chen, and T. Shun, “Wear Resistance and High-Temperature Compression Strength of Fcc CuCoNiCrAl ^ s ...,” Library (Lond)., no. May, 2004.
[5] T. Yang et al., “Precipitation behavior of Al x CoCrFeNi high entropy alloys under ion irradiation,” Sci. Rep., vol. 6, no. 1, p. 32146, 2016.
[6] H. Hadraba et al., “Oxide dispersion strengthened CoCrFeNiMn high-entropy alloy,” Mater. Sci. Eng. A, vol. 689, no. December 2016, pp. 252–256, 2017.
[7] X. Liu, H. Yin, and Y. Xu, “Microstructure, mechanical and tribological properties of Oxide Dispersion Strengthened high-entropy alloys,” Materials (Basel)., vol. 10, no. 11, 2017.
[8] J. S. Benjamin, “Dispersion strengthened superalloys by mechanical alloying,” Metall. Trans., vol. 1, no. 10, pp. 2943–2951, 1970.
[9] E. Gil, J. Cortés, I. Iturriza, and N. Ordás, “XPS and SEM analysis of the surface of gas atomized powder precursor of ODS ferritic steels obtained through the STARS route,” Appl. Surf. Sci., vol. 427, pp. 182–191, 2018.
[10] B. Gludovatz, A. Hohenwarter, D. Catoor, E.H. Chang, E.P. George, R.O. Ritchie, A fracture-resistant high-entropy alloy for cryogenic applications, Science 345 (2014) 1153e1158
[11] G. K. Williamson and W. H. Hall, “Discussion of the Theories of Line Broadening,” Acta Metall., vol. 1, p. 22, 1953.
[12] Halder, N. C., & Wagner, C. N. J. (1966). Separation of particle size and lattice strain in integral breadth measurements. Acta Crystallographica, 20(2), 312-313.
[13] Williamson, G. K., & Smallman, R. E. (1956). Philos. Mag.